Meridional contrasts in productivity changes driven by the opening of Drake Passage

Jean-Baptiste Ladant[1,2,3*], Yannick Donnadieu[1,4], Laurent Bopp[2,3], Caroline H. Lear[5], Paul A. Wilson[6]

*Corresponding author. Email: jbladant@gmail.com

[1]Laboratoire des Sciences du Climat et de l'Environnement, LSCE-IPSL, CEA / CNRS / UVSQ, Université Paris-Saclay, Gif-sur-Yvette, France.

[2]Ecole Normale Supérieure, Département de Géosciences, Paris, France.

[3]LMD / IPSL, CNRS / ENS / Ecole Polytechnique / UPMC, Paris, France.

[4]Aix Marseille Université, CNRS, IRD, Coll. France, CEREGE, Aix-en-Provence, France.

[5]School of Earth and Ocean Sciences, Cardiff University, Cardiff, UK.

[6]Ocean and Earth Science, National Oceanography Centre Southampton, University of Southampton, Southampton, UK.

Keypoints

- Productivity changes following Drake Passage opening are explored using the IPSL model and compared with data from the late Eocene and early Oligocene.
- Drake Passage opening drives a decrease in productivity in the low latitudes and spatially heterogeneous patterns in the high latitudes.
- Agreement between proxy records and model results indicate that Drake Passage opening has driven part of the late Eocene productivity changes.

Abstract

Changes in atmospheric pCO_2 are widely suggested to have played a major role in both the long-term deterioration of Cenozoic climate and many superimposed rapid climate perturbations such as the pivotal Eocene-Oligocene transition. Changes in marine productivity affecting the biological oceanic carbon pump represent one possible cause of past CO_2 variability. Here, we explore the relationship between ocean gateway change and marine biogeochemistry. Specifically, we use a fully coupled atmosphere-ocean-biogeochemical model (IPSL-CM5A) to examine global ocean paleoproductivity changes in response to the opening of Drake Passage. In our simulations, we find that Drake Passage opening yields a spatially uniform decrease in primary productivity in the low latitude oceans while the high latitude response is more spatially heterogeneous. Mechanistically, the low latitude productivity decrease is a consequence of a fundamental reorganization of ocean circulation when Drake Passage opens driven by the isolation of the Southern Ocean from low latitude water masses. Nutrient-depletion in the low latitudes is driven by a marked decrease in the intensity of deep convection in the Southern Ocean, which drives the accumulation of nutrients at depth and their depletion in the intermediate and upper ocean, especially away from sites of subduction. In the high latitudes, the onset of the Antarctic Circumpolar Current in the model exerts a strong control both on nutrient availability but also on regions of deep-water formation. The qualitative agreement between geographically diverse long-term paleoproductivity records and the simulated variations suggests that Drake Passage opening may contribute to the long-term paleoproductivity signal.

Introduction

Tectonic opening of Southern Ocean gateways constitutes one of the most fundamental changes in Cenozoic boundary conditions because of the capacity to alter global ocean circulation and climate [*Barker and Burrell*, 1977; *Kennett*, 1977]. In a seminal paper, *Kennett* [1977] proposed that the opening of these gateways (Drake and Tasman Passages) to deep circulation was instrumental in initiating sustained Antarctic glaciation. This sequence of events is suggested to have initiated during the late Eocene [*Matthews and Poore*, 1980; *Miller et al.*, 1991; *Lear et al.*, 2000; *Stickley et al.*, 2004; *Lagabrielle et al.*, 2009], although debate is ongoing about the timing of full gateway opening to a deep and wide current system [*Barker et al.*, 2007; *Katz et al.*, 2011; *Scher et al.*, 2015]. This appealing hypothesis suggests that the opening of Drake Passage (DP) and of the Tasman gateway would have engendered the onset of an Antarctic Circumpolar Current (ACC), thermally isolating the Antarctic continent from water masses sourced in the lower latitudes and permitting the growth of an extensive Antarctic ice sheet (AIS). However, this ocean gateway hypothesis has subsequently lost some ground because the results of numerical model experiments have been unable to robustly demonstrate that the sole climatic impact of DP (or Tasman gateway) opening was sufficient to initiate the glaciation [*Mikolajewicz et al.*, 1993; *DeConto and Pollard*, 2003; *Huber and Nof*, 2006; *Sijp et al.*, 2011; *Goldner et al.*, 2014]. Instead, modelling studies have pointed to a CO_2 decline as the primary driver of AIS initiation through atmospheric radiative cooling [*Mikolajewicz et al.*, 1993; *DeConto and Pollard*, 2003; *Huber et al.*, 2004]. The remarkable match between observations [*Coxall et al.*, 2005; *Coxall and Wilson*, 2011] and model predictions [*DeConto and Pollard*, 2003; *Ladant et al.*, 2014] of the structure of the deep sea oxygen isotope record across the Eocene-Oligocene transition (EOT) and paleo-CO_2 reconstructions for this interval [*Pearson et al.*, 2009; *Pagani et al.*, 2011; *Heureux and Rickaby*, 2015] lend support to the CO_2 hypothesis. Yet these CO_2

reconstructions are far from well-developed and the influence of ocean gateway opening and CO_2 forcing need not be mutually exclusive [*Egan et al.*, 2013; *Lear and Lunt*, 2016; *Elsworth et al.*, 2017].

There exists a rich literature documenting long-term changes in oceanic carbon cycling associated with Cenozoic climate deterioration including across the pivotal EOT thanks to scientific ocean drilling [e.g., *Siesser*, 1995; *Schumacher and Lazarus*, 2004; *Faul and Delaney*, 2010; *Griffith et al.*, 2010; *Coxall and Wilson*, 2011; *Pälike et al.*, 2012; *Egan et al.*, 2013; *Moore et al.*, 2014; *Plancq et al.*, 2014; *Villa et al.*, 2014]. Paleoproductivity reconstructions from the data – taken here to mean export production of organic matter to the deep ocean since most paleo data studies inherently quantify export production rather than primary productivity – display spatially heterogeneous long-term variations between the late Eocene and the Oligocene (Table 1). Data from the northern high-latitudes are lacking but records from the southern high-latitudes generally document paleoproductivity increases from the Eocene into the Oligocene [*Schumacher and Lazarus*, 2004; *Plancq et al.*, 2014; *Villa et al.*, 2014] while the low latitudes record a general decrease [*Schumacher and Lazarus*, 2004; *Griffith et al.*, 2010; *Moore et al.*, 2014].

Numerical modelling studies have investigated the role of DP opening on global ocean circulation and climate with spatially resolved Earth system models [*Mikolajewicz et al.*, 1993; *Toggweiler and Bjornsson*, 2000; *Sijp and England*, 2004; *Sijp et al.*, 2009; *Zhang et al.*, 2010; *Sijp et al.*, 2011; *Yang et al.*, 2014; *Fyke et al.*, 2015; *England et al.*, 2017]. In contrast, modelling of ocean biogeochemical changes across the late Eocene and Oligocene has been limited. Most work of this type has been undertaken using either numerical box models focusing specifically on the Eocene-Oligocene Transition itself [*Zachos and Kump*, 2005; *Merico et al.*, 2008; *Armstrong McKay et al.*, 2016] or using the UVic earth system model of intermediate complexity (EMIC) integrating a biogeochemical component [*Pagani*

100 *et al.*, 2011; *Fyke et al.*, 2015]. Box models are powerful tools to investigate the credibility of
101 competing hypotheses at the global scale but they cannot be used to confront localized
102 paleoproductivity reconstructions. On the other hand, results from experiments using the
103 UVic EMIC suggest that the successive opening of DP and of the Panama seaway through
104 Cenozoic time would have exerted a major influence on the inter-basin carbon reservoir and
105 in setting the modern dissolved inorganic carbon gradients between basins [*Fyke et al.*, 2015].
106 *Pagani et al.* [2011] utilize an Eocene UVic simulation to generate Eocene-Oligocene surface
107 ocean phosphate concentrations, which they further use to compute surface ocean CO_2
108 concentrations to ultimately constrain their reconstructions of atmospheric CO_2 across the
109 EOT. Their results also suggest that, compared to modern, the surface ocean phosphate
110 concentration increases in the low latitudes and decreases in the high latitudes.
111 Here, we revisit the question of the biogeochemical impacts of DP using a more
112 sophisticated, fully coupled, IPCC-class model with, for the first time, a focus on
113 paleoproductivity changes and we compare our results with long-term records of productivity
114 change from the late Eocene to Oligocene. It should be noted that *Winguth et al.* [2012] also
115 applied a fully-coupled IPCC-class GCM to investigate paleoproductivity changes during the
116 Eocene, but their focus was the PETM and as such they realized simulations at different CO_2
117 rather than with open or closed gateways. Assessing the role DP opening played in driving
118 paleoproductivity changes during the late Eocene and Oligocene is important because of its
119 influence on the global carbon cycle and in particular pCO_2 variations, via changes in the
120 oceanic biological pump (see *Hain et al.* [2014] for a review). In the following, we explore
121 the effects of opening DP on long-term productivity changes using a similar approach to that
122 of *Fyke et al.* [2015] and *Elsworth et al.* [2017] in that we employ continental and
123 bathymetric configurations altered from those of present-day. In this respect, strictly speaking,
124 our experiment is a paleogeography sensitivity simulation rather than a simulation of Eocene-

Oligocene events. Nevertheless, our approach allows us to isolate the effect of DP opening on global climate and productivity and to make a semi-quantitative comparison to proxy records. Here we focus on comparing our results to records spanning the late Eocene and early Oligocene – the canonical interval for which DP opening is invoked as a climate forcing mechanism – but the possibility that a fully developed ACC was only established during the late Miocene [e.g., *Dalziel et al.*, 2013] also lends our results a longer-term Cenozoic relevance.

Models

The results presented in this study are obtained with the IPSL-CM5A Earth System Model [*Dufresne et al.*, 2013], which includes both a representation of the physical atmosphere-ocean-land-sea ice interactions and of the global carbon cycle. Its configuration combines the atmospheric model LMDz [*Hourdin et al.*, 2013], the land-surface model ORCHIDEE [*Krinner et al.*, 2005] and the ocean model NEMOv3.2 [*Madec*, 2008]. The OASIS coupler [*Valcke*, 2006] is used to interpolate and exchange variables and synchronize the models [*Dufresne et al.*, 2013]. Only succinct details about the models will be given here because their full description can be found in *Dufresne et al.* [2013] (see also *Kageyama et al.* [2013] for a description of the model used in paleo configurations for the Last Glacial Maximum and the mid-Holocene). LMDz solves the equation of atmospheric motion on a regular longitude-latitude grid using σ-P vertical coordinates. The resolution used in this study is 96x95x39 (lon. x lat. x vert.), corresponding to 3.75° of longitude and 1.875° of latitude, and 39 vertical levels irregularly distributed. ORCHIDEE runs on the same grid as LMDz and contains a land-surface scheme that simulates both the energy and water cycles of soils and vegetation and a routing scheme that routes precipitated water to the ocean. 12 Plant Functional Types (PFT) define the vegetation. Although the vegetation cover is imposed in

this version of IPSL-CM5A, the PFT phenology is computed interactively given the atmospheric state simulated by LMDz. The NEMO model comprises an ocean dynamics component (OPA, *Madec* [2008]), a thermodynamic-dynamic sea-ice model (LIM2, *Fichefet and Morales Maqueda* [1997]), and an ocean biogeochemistry model (PISCES, *Aumont and Bopp* [2006]). NEMO uses a tripolar grid in order to avoid North Pole singularity [*Madec and Imbard,* 1996], for both dynamics and physics. It has a nominal latitudinal resolution of 2°, increasing up to 0.5° at the Equator, and a longitudinal resolution of approximately 2° and 31 unequally spaced vertical levels, the thickness of which varies from 10 m near the surface to 500 m at the bottom. PISCES includes a simple representation of the marine ecosystem and of the main oceanic biogeochemical cycles [*Aumont and Bopp*, 2006]. It explicitly represents two classes of phytoplankton (nanophytoplankton and diatoms), two classes of zooplankton, five pools of nutrients (phosphate, nitrate, silicic acid, ammonium and iron), two classes of particulate organic carbon (small and large) and semi-labile dissolved organic carbon. It also includes dissolved and particulate inorganic carbon, alkalinity and dissolved oxygen. The main biogeochemical interactions, such as photosynthesis, respiration, grazing, particle aggregation and sinking, and remineralization, dictate the spatio-temporal evolution of each pool with respect to each other. Phytoplankton growth is limited by the aforementioned nutrients and by light availability. Ratios of C:N:P in the organic pools are kept constant following *Takahashi et al.* [1985], whereas Fe:C ratios for both phytoplankton classes and Si:C ratios for diatoms are prognostically simulated as a function of the external concentration of nutrients and light availability [*Aumont and Bopp*, 2006]. The full description of the version of PISCES used in this study can be found in *Aumont and Bopp* [2006]. All these models have been validated and used, either separately or together within the IPSL-CM5A model, over a variety of climates that include pre-Quaternary climates [e.g., *Contoux et al.*, 2015; *Tan et al.*, 2017], LGM [e.g., *Mariotti et al.*, 2012; *Kageyama et al.*, 2013],

preindustrial [*Le Mézo et al.*, 2017] and present-day and future climates [e.g., *Aumont and Bopp*, 2006; *Bopp et al.*, 2013; *Tagliabue et al.*, 2014], including the latest IPCC exercise.

In a first step, two simulations are run with the fully coupled IPSL-CM5A model. Both simulations have a preindustrial land-sea mask, from which the geometry of the Panama Seaway has been altered to represent mid-Cenozoic tectonic configurations (in practice, this means replacing continental grid points by oceanic grid points, see Supplementary Fig. 1). In addition, the land-sea mask of the first simulation, named DC (for Drake Closed), has been modified to add terrestrial points at the Drake Passage to simulate its closure. Conversely, the Drake Passage is left unchanged from that of the preindustrial in the land-sea mask of the second simulation, named DO (Drake Opened). Compared to preindustrial conditions, ice sheets over polar continents have been removed and replaced by tundra-like vegetation but otherwise the preindustrial vegetation cover is kept for both simulations. The ocean is initialized as homogeneous in salinity (34.5 $kg.m^{-3}$) and with surface temperature following a latitudinal profile ranging from 9°C at the poles to 36°C at the equator. The deep ocean is initialized at a uniform temperature of 7°C (Supplementary Fig. 2). There is no sea ice at the beginning of the simulations. We prescribe a CO_2 concentration of 1120 ppm, which is consistent with most of the records of paleo-CO_2 levels for the Eocene [*Beerling and Royer*, 2011] and justifies the absence of ice sheets over the poles because the inception of ice over Antarctica is thought to occur at lower CO_2 levels [*Gasson et al.*, 2014; *Ladant et al.*, 2014; *Heureux and Rickaby*, 2015]. Each of the two experiments is run for 1000 years. We acknowledge here that longer integrations (>= 3000 years) are desirable but we are precluded by the computational performances of this version of the IPSL-CM5A model. However, after 1000 years, the surface ocean is in equilibrium and the very small residual trend (< 0.1 °C/century) that exists in the deep ocean is unlikely to significantly affect the outcomes of the study.

Oceanic biogeochemical equilibrium typically requires longer simulations to be attained than the dynamical equilibrium [*Séférian et al.*, 2016]. In a second step, we run offline simulations of the PISCES model in order to be closer to the biogeochemical equilibrium. PISCES is initialized with the oceanic biogeochemical outputs from the last year of DC and DO coupled experiments and forced by the ocean dynamical fields of DC and DO. In detail, the last 100 years of ocean dynamics outputs are passed to PISCES-offline in a repetitive sequence (that is, after each 100 years of simulation, the ocean forcing is repeated for the next 100 years). The simulations DC-P (for DC-PISCES) and DO-P are run for 2000 years to ensure equilibrium of the biogeochemical fields. One caveat must be noted here. In this version of IPSL-CM5A, the nutrient delivery to the ocean is fixed. This is an important simplification because under different climates the global amount of nutrients as well as the spatial distribution of nutrient inputs to the ocean (i.e., the intensity and location of the river flows) will be altered. However, as our purpose is to isolate the climatic and biogeochemical effects of DP opening only and to provide insights into its long-term signature in the proxy record, we have kept present-day nutrient inputs in the simulations.

In the following, we refer to the closed (open) Drake Passage simulations by DC (DO) regardless of whether we consider the fully coupled IPSLCM5A or the PISCES-offline simulation, but dynamical results utilize the IPSLCM5A simulations while the biogeochemistry is discussed using the PISCES-offline simulations.

Results

In the simulations, the opening of DP significantly alters paleoproductivity (i.e., paleo export production). Figure 1 shows the DC and DO global annual export production of organic carbon at 100 m, a commonly used measure of the carbon export into the deep ocean. The major areas contributing to this export are similar in the two simulations (Fig. 1) but in

regions such as the low latitude Indian and Pacific oceans, productivity uniformly decreases with DP opening (Figs. 1 and 2). In contrast, in the Southern Ocean, while productivity decreases in the Atlantic sector, it increases in the Pacific and Indian sectors when DP opens. In the zonal average, opening DP yields an increase in carbon export to the deep ocean in the southern high latitudes but a decrease in the low latitudes and northern high latitudes. This dipole pattern of increase in the southern high latitudes and decrease in the low latitudes agrees with the meridional contrast seen in the data (Table 1). The spatial pattern of increase/decrease in our simulations also compares favourably with observations from various drilling locations (Fig. 1).

The observed patterns of paleoproductivity change are the consequence of alterations in ocean circulation, which controls the supply of nutrients, essentially nitrate and phosphate, brought from the deep or sub-surface ocean to the surface. The zonally averaged redistribution of nutrients follows a dipole pattern on the vertical (Fig. 3) with a decrease in the intermediate and upper ocean and an increase at depth when DP opens, except in the highest latitudes of the Southern Ocean (> 60°S). Indeed, in this region, an increase in the concentration of nutrients occurs throughout the whole water column when DP opens. Vertical gradients in the upper 500 m confirm the decreased nutrient availability in the low latitudes of each basin in DO and the increase in the southern high latitudes (Fig. 4), except in the upper 100 m of the Atlantic sector.

The redistribution of nutrients in our simulations directly follows the reorganization of the oceanic thermohaline circulation (Figs. 5 and 6). In DC, the circulation is dominated by a vigorous Southern Hemisphere overturning cell of up to 30 Sv (Fig. 5), which is fed via deep convection (> 2000 m) in the Pacific and Atlantic sectors of the Southern Ocean (Fig. 6). These deep waters then fill the deep ocean globally, circulate northward in the abyss, are strongly upwelled in the low latitudes at depth and return southward between 500 m and 1500

m depth. There is no deep-water formation in the Northern Hemisphere and the closed DP prevents the existence of a well-developed ACC. A wind-driven circumpolar circulation still develops around Antarctica under the influence of the Westerlies (Supplementary Fig. 3), which generates upwelling cells carrying waters from the southward branch of the overturning circulation to the surface. Some of these waters then feed the abyssal circulation through deep convection around Antarctica while the remaining fraction is advected northward to feed intermediate and modal ocean circulation [*Toggweiler and Samuels*, 1993]. The absence of a well-developed ACC leads to enhanced export of warm and salty subtropical waters into the Southern Ocean, increasing the intensity of deep water formation there as well as the southward ocean heat transport [*Sijp and England*, 2004].

Opening DP strongly modifies the global ocean circulation (Fig. 5). Arguably, the major difference lies in the appearance of a vigorous modern-like ACC (Supplementary Fig. 3), which interconnects the three major basins from top to bottom and generates a relatively deep Deacon Cell (~ 2000 m), which reflects the existence of deep upwelling cells. The latter are deeper and more expanded towards Antarctica relative to DC, as shown by the overlain isopycnals on Figs. 3a and 3b, and then feed the abyssal and the intermediate/modal circulations as in DC. Abyssal waters formed around Antarctica remain however mostly confined below 2000 m (Fig. 5). The existence of a well-developed ACC limits the advection of warm and salty subtropical waters to the Southern Ocean, which reduces the intensity of deep convection (Fig. 6) because at high latitudes, salinity exerts the dominant control over the stratification of ocean waters [*Ferreira et al.*, 2010; *Yang et al.*, 2014]. A very weak overturning cell appears in the Nordic Seas, promoting modest intermediate water formation (up to ~ 700 m, Fig. 6). The rates of global overturning in DO are thus greatly reduced relative to DC, increasing the residence time of water in the deep ocean.

The transition from a well-ventilated DC to a more stagnant DO ocean thereby drives accumulation of nutrients at depth and depletion in the intermediate and upper ocean in DO relative to DC because the reduced ventilation acts to 'de-homogenize' the ocean (Fig. 3c). In DC, the much stronger abyssal low latitudes upwelling allow nutrients to be more rapidly exported in the vigorous southward branch of the overturning circulation whereas in DO, these nutrient-rich waters are confined below 2000 m, thus increasing the nutrient concentrations below 2000 m and decreasing them above 2000 m in DO relative to DC.

In both simulations, nutrient-enriched waters are then carried to the surface by the Southern Ocean upwelling cells (Figs. 3a and 3b) but because of the intensity and shape of the overturning circulation, the upwelled waters contain more nutrients in DC relative to DO. This is why the subsurface nutrient concentrations between 40°S and 60°S decrease in DO. However, because the upwelling cells are deeper and expand slightly southward in DO, the subsurface of the highest latitude oceans (> 60°S) is enriched in nutrients relative to DC (Figs. 3c and 4, again except for the upper 100 m in the Atlantic sector).

The decrease in subsurface nutrient concentration in the 40°S-60°S area in DO has important consequences for the low latitude nutrient supply. Indeed, the intermediate and modal waters (IMW) formed in this area are then advected to feed low latitude subsurface waters [*Toggweiler and Samuels*, 1993; *Sarmiento et al.*, 2004]. Because the IMW are poorer in nutrients when DP is open, the supply of nutrients to the low latitudes decreases. In addition, the slight increase in the tilt of the isopycnals in DO between 40°S and 50°S indicates that IMW sink deeper than in DC and consequently may contribute to the decrease in nutrient supply to the subsurface low latitudes waters in DO.

While low latitude productivity and export changes are well explained by the decreased nutrient availability resulting from the less dynamic DO ocean, additional processes contribute to the modelled changes in productivity in the Southern Ocean. Indeed, convective

mixing, associated with deep-water formation in winter and wind-driven circumpolar currents, heavily influences export productivity patterns at these latitudes (Figs. 1 and 6). In the Pacific sector, the DO deep-water convective areas are significantly shallower and narrower but remain deep enough to increase the productivity because the convection affects water masses significantly enhanced in nutrients. Following the onset of the ACC, a large convection zone appears in the southern Indian Ocean around 50°S, which, albeit relatively shallow (up to 500 m), drives a large increase in productivity (Fig. 1). Similarly, the wider convection zone just offshore Antarctica at the longitude of Africa generates productivity increase. Finally, in the Atlantic sector, the opposite occurs. Deep-water convection is completely shut down in DO in the central South Atlantic Ocean, leading to a substantial area of decreased productivity.

Because the PISCES model allows the explicit representation of nanophytoplankton and diatoms, we can also assess the role of these different groups in driving the modelled primary productivity changes (Fig. 7 and Supplementary Fig. 4). In the low latitudes, the decrease in primary productivity is essentially driven by a strong decline in nanophytoplankton productivity whereas diatom productivity, even if contributing much less to the total, remains relatively stable (except in the coastal Indian ocean). In contrast, in the mid- and high-latitudes, diatoms are responsible for a large part of primary productivity changes, and even become the main contributor to productivity changes in the highest latitudes (> 60°S). This is consistent with increased nutrient availability in the highest latitudes of the DO simulation due to the onset of the ACC. For instance, in the South Pacific, even if winter convection zones are shallower and narrower, the enhanced nutrient supply favours diatoms over nanophytoplankton.

Discussion

1. Comparison to model simulations

Numerous studies have investigated the role of DP on global climate, with varying continental configurations [e.g., *Mikolajewicz et al.*, 1993; *Heinze and Crowley*, 1997; *Toggweiler and Bjornsson*, 2000; *Sijp and England*, 2004; 2005; *Zhang et al.*, 2010; *Sijp et al.*, 2011; *Yang et al.*, 2014; *England et al.*, 2017]. Of these, the most relevant simulations to our study are those performed with the same continental configuration, in particular with the Panama seaway open [e.g., *Mikolajewicz et al.*, 1993; *Yang et al.*, 2014; *Fyke et al.*, 2015]. Our reasoning here is based on the results of *Yang et al.* [2014] who demonstrated that the impacts of DP are strongly dependant upon the configuration of the Panama seaway. Using the CM2Mc model in a modern configuration (thus a closed Panama seaway), they show that the closure of DP leads to an ocean circulation resembling that of modern, with the notable exception of the suppression of the Antarctic Bottom Water cell in the Atlantic Ocean. This result is broadly confirmed by *England et al.* [2017], in which the same experiment with the fully coupled CSIRO Mk3L model demonstrates that the DP closed configuration exhibits similar rates of NADW and AABW relative to modern. On the contrary, with an open Panama seaway in an otherwise modern continental configuration, *Yang et al.* [2014] show that the closure of DP generates a large and wide Southern overturning cell and suppresses northern sinking. Our results, obtained with an open Panama seaway, are in agreement with the findings of *Yang et al.* [2014], but also with those of *Fyke et al.* [2015] and *Mikolajewicz et al.* [1993] who find a similar ocean circulation with a closed Drake – open Panama configuration, albeit with simpler models (EMIC or ocean-only models).

Ocean circulation in the presence of an open DP and an open Panama seaway (i.e., the impact of the opening of Panama) has also received considerable attention [e.g., *Mikolajewicz et al.*, 1993; *Lunt et al.*, 2008; *Sepulchre et al.*, 2014; *Yang et al.*, 2014; *Fyke et al.*, 2015]. All models ventilate the deep ocean from the South, although with reduced intensity than with a

closed DP, whereas the rates of deep-water formation in the North vary greatly between studies. *Yang et al.* [2014] find virtually no difference between a DO configuration with or without an open Panama seaway, that is, in both cases a strong NH deep overturning cell. In their simulations with the UVic model, *Fyke et al.* [2015] obtain a significant reduction in rates of NH deep water formation with an open Panama Gateway, albeit not a shutdown. A similar result is obtained by *Sepulchre et al.* [2014] with the IPSL-CM4 model and by *Lunt et al.* [2008] with the HadCM3 model. On the contrary, *Mikolajewicz et al.* [1993] find, with the ocean-only Hamburg model, that a Drake open and Panama open configuration leads to the cessation of the formation of NADW. In our runs, the thermohaline circulation induced by the DO configuration shows a weak NH intermediate water formation, which is close to the no-NADW state of *Mikolajewicz et al.* [1993]. It is interesting to note that the existence and vigour of the NADW rates in these different models might, at least in part, be driven by the geometry and size of the Panama gateway. Indeed, when Panama is closed (i.e. the modern state), all models show NADW formation. Models run with an open but narrow Panama seaway show reduced rates of NADW formation [*Lunt et al.*, 2008; *Sepulchre et al.*, 2014; *Fyke et al.*, 2015] and those run with a wide Panama seaway show NADW shutdown [*Mikolajewicz et al.*, 1993; this study]. Support for this finding comes from the simulations of *Sijp et al.* [2009] and *Sijp et al.* [2011]. In the first of these studies, open and closed DP simulations are performed in a modern continental configuration, that is, with a closed Panama seaway. Their DP open simulations yield significant NADW formation. In the second of these studies, coupled opening of DP and the Tasman gateway is simulated with the Eocene configuration of *Huber et al.* [2003], which features a wide Panama seaway. Interestingly, no NADW forms in these simulations. The simulations of *Yang et al.* [2014] yield contrasting results, however, because, with DP open, vigorous NADW rates exist regardless of whether a wide or a closed Panama seaway is prescribed. We tentatively infer

that the different boundary conditions (pCO_2 and ice sheets cover for instance) applied by *Yang et al.* [2014] and in our study may play a role. In particular, the effect of pCO_2 on ocean circulation may explain part of the discrepancy between the strong NADW rates found in the fully coupled GCM used by *Yang et al.* [2014] and our weak intermediate water formation state (see discussions in *Lunt et al.* [2010], *Donnadieu et al.* [2016] and *Winguth et al.* [2012]). In this regard, it is also interesting to note that the no-NADW simulations of *Sijp et al.* [2011] are run, as in our study, with elevated pCO_2. Another factor that should not be ignored is that our fully coupled 1000 year GCM simulations can only be considered to have reached quasi-equilibrium and may miss further reorganizations of ocean circulation. However, although the Northern Hemisphere thermohaline state of the ocean differs between studies, we note that the dynamical results produced by our simulations are consistent with previous findings in that the opening of DP isolates Antarctica from warm and salty subtropical waters, which acts to freshen and cool most of the surface Southern Ocean (Supplementary Fig. 5). We conclude this climatic comparison by acknowledging that many important studies involving the opening of DP (or Tasman gateway) have been carried out using Eocene boundary conditions [e.g., *Huber et al.*, 2003; *Huber et al.*, 2004; *Huber and Nof*, 2006; *Zhang et al.*, 2010; *Sijp et al.*, 2011] but the idealized character of our modelling setup makes a direct comparison with these studies more questionable.

Two previous numerical studies are particularly relevant to our findings because they numerically address the impact of gateways opening on the biogeochemical state of the ocean, using the spatially resolved, albeit simpler, UVic climate-biogeochemical model [*Pagani et al.*, 2011; *Fyke et al.*, 2015]. In line with the findings of *Fyke et al.* [2015] (their figure 9), opening DP in our simulations increases DIC concentrations at depth in all basins although we do not observe a shift from a higher Atlantic DIC concentration to a higher Pacific DIC concentration (not shown). Our results also broadly agree with those of *Pagani et al.* [2011]

399 who show that the surface phosphate concentration in their Eocene simulation features a
400 spatially uniform increase in the low latitudes and decrease in the southern high latitudes
401 relative to modern, attributed to the shallower Eocene Southern Ocean upwelling cells relative
402 to modern induced by the gateways configurations. However, in our experiments, the changes
403 in surface nutrient concentrations in the southern high-latitudes are heterogeneous with areas
404 of increase and decrease. Because we can unambiguously attribute the reorganization of
405 surface nutrient concentration to DP opening in our simulations, we speculate that the
406 gateways impact in the work of *Pagani et al.* [2011] is intertwined with other drivers, such as
407 the much higher CO_2 concentration and other geographical characteristics imposed in their
408 Eocene run relative to their modern.
409
410 2. Comparison to observations
411 Many data studies have investigated paleoproductivity changes during the Eocene and
412 Oligocene [e.g., *Siesser*, 1995; *Diester-Haass and Zahn*, 1996; *Salamy and Zachos*, 1999;
413 *Diester-Haass and Zahn*, 2001; *Diester-Haass and Zachos*, 2003; *Nilsen et al.*, 2003;
414 *Schumacher and Lazarus*, 2004; *Dunkley Jones et al.*, 2008; *Griffith et al.*, 2010; *Coxall and*
415 *Wilson*, 2011; *Egan et al.*, 2013; *Moore et al.*, 2014; *Plancq et al.*, 2014; *Villa et al.*, 2014]
416 but the imprint of tectonics, particularly DP opening, is complex to decipher unambiguously
417 because other climatic shifts, such as the EOT glaciation, occur contemporaneously.
418 However, by investigating exclusively the effects of DP opening in a warmer world, our
419 simulations provide insights on this possible imprint. It is particularly interesting to note that,
420 when compared to records that span an interval longer than the EOT glaciation event, model
421 results are qualitatively consistent with data (Fig. 1), suggesting that, if the DP was
422 sufficiently well breached by the early Oligocene, at least part of the long-term
423 paleoproductivity signal recorded in the data may be attributed to its opening. Our results

suggest that DP opening drove a significant reduction in paleoproductivity in the low latitude oceans – a finding consistent with long-term recorded changes, especially in the Eastern Equatorial Pacific [*Schumacher and Lazarus*, 2004; *Moore et al.*, 2014] and in the Equatorial Indian Ocean [*Siesser*, 1995]. In the high latitudes, most long-term records document an increase in paleoproductivity [e.g., *Diester-Haass and Zahn*, 1996; 2001; *Schumacher and Lazarus*, 2004], but the pattern of paleoproductivity increase/decrease simulated by the model is not uniform and strongly related to variations in the convective mixing areas.

Our simple model-data comparison is similar to that of *Winguth et al.* [2012]. A more in-depth analysis is unwarranted because we present a paleogeography sensitivity simulation rather than an attempt to simulate Eocene-Oligocene events *sensu stricto*. Furthermore, different data sets produce sometimes contrasting indications of paleoproductivity change even when taken from the same site. A good example comes in the paleoproductivity records from the Eastern Equatorial Pacific [e.g., *Coxall and Wilson*, 2011; *Erhardt et al.*, 2013; *Moore et al.*, 2014]. Although there are reasonable explanations to these discrepancies [*Erhardt et al.*, 2013; *Moore et al.*, 2014], this observation highlights the complexity associated with reconstructing paleoproductivity from proxy signals [*Anderson and Delaney*, 2005]. In the high latitudes, many records show significant enhancement of the paleoproductivity during the EOT event [e.g., *Salamy and Zachos*, 1999; *Diester-Haass and Zahn*, 2001; *Plancq et al.*, 2014; *Villa et al.*, 2014] or during the latest Eocene [*Diekmann et al.*, 2004; *Egan et al.*, 2013; *Villa et al.*, 2014]. In particular, during the latter, it has been argued that pulses of tectonic opening of DP [*Scher and Martin*, 2006] may play a role in the transition from oligotrophic to eutrophic nannofossils taxa [*Villa et al.*, 2014] or an increase in diatom abundance [*Egan et al.*, 2013]. Based on Si isotopes records, *Egan et al.* [2013] invoke increased diatom primary productivity to explain the recorded increased silicic acid utilization at the surface at Site 1090. Although our modelled results support a net decrease in

449 diatoms (and nanophytoplankton) primary production in most of the South Atlantic Ocean
450 (Fig. 7), the simulated export production increases at Sites 689 [*Villa et al.*, 2014] and 1090
451 [*Egan et al.*, 2013]. Primary and export productivity do indeed not necessarily co-vary as
452 organic matter remineralization, among others, is a function of temperature [*John et al.*,
453 2013]. The significant modelled surface cooling when DP opens at Sites 689 and 1090
454 (Supplementary Fig. 5) generates reduced recycling of organic matter and may thus explain
455 the contrasting variations of primary and export productivity.
456
457 3. Caveats related to the idealized framework of the study
458 Taken at face value, our simulated paleoproductivity changes fit marine records
459 reasonably well, but important caveats must be kept in mind when interpreting our model
460 results. First, we do not use a realistic late Eocene global paleogeography, either regarding the
461 geometry of important gateways or other major tectonic differences such as the existence of
462 the Tethys Sea or the position and height of the Tibetan Plateau. Our idealized simulations
463 therefore remain a sensitivity experiment to the opening of DP. Because our simulated
464 paleoproductivity changes are essentially driven by the onset of the ACC, the impact of a
465 closed or restricted Tasman seaway prior to the latest Eocene [*Huber et al.*, 2004; *Stickley et*
466 *al.*, 2004] may have important consequences for paleoproductivity patterns. However, a
467 recent idealized study suggests that a circumpolar water path, which would circumvent
468 Australia, could exist even in the absence of an open Tasman seaway [*Munday et al.*, 2015].
469 Second, our simulations were performed using two end-member boundary conditions (DP
470 closed and DP open) that are not strictly representative of the late Eocene and Oligocene, as
471 some evidence points to initial opening of DP as early as the Early Eocene [*Eagles et al.*,
472 2006; *Eagles and Jokat*, 2014]. The climatic relevance of an incipient opening is intuitively
473 questionable and the concept of a threshold relationship between gateway opening and

climate response is appealing. *Sijp and England* [2005] argued that the sill depth of DP critically impacted the global ocean circulation, because it was instrumental in controlling the formation of NADW, but this result was obtained with a closed Panama Seaway, which is a configuration that favours NADW formation [*Lunt et al.*, 2008; *Sepulchre et al.*, 2014; *Yang et al.*, 2014]. The open Panama simulations performed here are not sufficient to unambiguously answer this question. Finally, our offline PISCES simulations are run with fixed nutrient supply from rivers, which are unaffected by variations in runoff whereas we know that changes in nutrient and carbonate supply down rivers across the Eocene Oligocene Transition are both likely and capable of driving major change in global carbon cycling [*Coxall et al.*, 2005; *Dunkley Jones et al.*, 2008; *Merico et al.*, 2008; *Armstrong McKay et al.*, 2016].

Conclusion

Using the IPSL-CM5A coupled model we have shown that the opening of Drake Passage profoundly alters oceanic paleoproductivity patterns across the globe. The reorganization of the oceanic circulation, from a well-ventilated ocean when Drake Passage is closed to a more stagnant state when Drake Passage is open, drives subsurface nutrient depletion in the low latitudes. Nanophytoplankton, rather than diatoms – possibly because the latter are only marginal contributors to the modelled low latitude primary productivity, are strongly affected by this depletion and the productivity consequently declines, especially in the Pacific and Indian oceans. In the high latitudes, productivity changes are driven both by nutrient availability and areas of convective mixing, which generate zones of productivity increase (most of the southern Pacific and Indian oceans) and decrease (most of the South Atlantic Ocean). In contrast to the low latitudes, diatoms are largely responsible for these productivity variations, especially in the southernmost latitudes. A simple qualitative

comparison with geological records reveals a good match between locations of paleoproductivity changes simulated by the model and inferred from data, suggesting that the role of Drake Passage opening in driving part of the long-term productivity signal across the late Eocene and early Oligocene may be non-negligible.

Acknowledgements

We are grateful to J.R. Toggweiler, Willem Sijp and Matt Huber for their insightful comments, and to Ellen Thomas for editorial handling. We thank the CEA/CCRT for providing access to the HPC resources of TGCC under the allocation 2014-012212 made by GENCI. We acknowledge the support of the project Anox-Sea funded by the ANR under the grant number ANR-12-BS06-0011-03. Long-term storage of the initial and boundary conditions and of the key climatological and biogeochemical outputs of the simulations will be performed at the LSCE storage system and/or at the TGCC storage system. We acknowledge use of the Panoply (www.giss.nasa.gov/tools/panoply/) and Ferret (ferret.pmel.noaa.gov/Ferret/) programs for analysis and graphics in this paper.

Author Contributions

J.-B.L. designed and performed the numerical simulations, with contributions from Y.D., and wrote the draft of the manuscript. All authors analysed and discussed the results and contributed to the final version of the manuscript.

Additional Information

The authors declare no competing financial interest. Correspondence and requests for materials should be addressed to either J.-B.L. (jbladant@gmail.com) or Y.D. (donnadieu@cerege.fr).

References

Anderson, L. D., and M. L. Delaney (2005), Middle Eocene to early Oligocene paleoceanography from Agulhas Ridge, Southern Ocean (Ocean Drilling Program Leg 177, Site 1090), *Paleoceanography*, *20*(1).

Armstrong McKay, D. I., T. Tyrrell, and P. A. Wilson (2016), Global carbon cycle perturbation across the Eocene‐Oligocene climate transition, *Paleoceanography*.

Aumont, O., and L. Bopp (2006), Globalizing results from ocean in situ iron fertilization studies, *Global Biogeochemical Cycles*, *20*(2).

Barker, P., and J. Burrell (1977), The opening of Drake passage, *Marine geology*, *25*(1), 15-34.

Barker, P. F., G. M. Filippelli, F. Florindo, E. E. Martin, and H. D. Scher (2007), Onset and role of the Antarctic Circumpolar Current, *Deep Sea Research Part II: Topical Studies in Oceanography*, *54*(21), 2388-2398.

Beerling, D. J., and D. L. Royer (2011), Convergent Cenozoic CO2 history, *Nature Geoscience*, *4*(7), 418-420.

Bopp, L., L. Resplandy, J. C. Orr, S. C. Doney, J. P. Dunne, M. Gehlen, P. Halloran, C. Heinze, T. Ilyina, and R. Seferian (2013), Multiple stressors of ocean ecosystems in the 21st century: projections with CMIP5 models, *Biogeosciences*, *10*, 6225-6245.

Contoux, C., C. Dumas, G. Ramstein, A. Jost, and A. M. Dolan (2015), Modelling Greenland ice sheet inception and sustainability during the Late Pliocene, *Earth and Planetary Science Letters*, *424*, 295-305.

Coxall, H. K., and P. A. Wilson (2011), Early Oligocene glaciation and productivity in the eastern equatorial Pacific: Insights into global carbon cycling, *Paleoceanography*, *26*(2).

Coxall, H. K., P. A. Wilson, H. Pälike, C. H. Lear, and J. Backman (2005), Rapid stepwise onset of Antarctic glaciation and deeper calcite compensation in the Pacific Ocean, *Nature*, *433*(7021), 53-57.

Dalziel, I. W. D., L. A. Lawver, J. A. Pearce, P. F. Barker, A. R. Hastie, D. N. Barfod, H. W. Schenke, and M. B. Davis (2013), A potential barrier to deep Antarctic circumpolar flow until the late Miocene?, *Geology*, *41*(9), 947-950.

DeConto, R. M., and D. Pollard (2003), Rapid Cenozoic glaciation of Antarctica induced by declining atmospheric CO2, *Nature*, *421*, 245-249.

Diekmann, B., G. Kuhn, R. Gersonde, and A. Mackensen (2004), Middle Eocene to early Miocene environmental changes in the sub-Antarctic Southern Ocean: evidence from biogenic and terrigenous depositional patterns at ODP Site 1090, *Global and Planetary Change*, *40*(3), 295-313.

Diester-Haass, L., and R. Zahn (1996), Eocene-Oligocene transition in the Southern Ocean: History of water mass circulation and biological productivity, *Geology*, *24*(2), 163-166.

Diester-Haass, L., and R. Zahn (2001), Paleoproductivity increase at the Eocene,ÄìOligocene climatic transition: ODP/DSDP Sites 763 and 592, *Palaeogeography, Palaeoclimatology, Palaeoecology*, *172*(1), 153-170.

Diester-Haass, L., and J. Zachos (2003), The Eocene-Oligocene transition in the Equatorial Atlantic (ODP Site 925); paleoproductivity increase and positive d13C excursion., in *From greenhouse to icehouse; the marine Eocene-Oligocene transition*, edited by D. R. Prothero, L. C. Ivany and E. A. Nesbitt, Columbia University Press, New York, NY, USA.

595 Donnadieu, Y., E. Pucéat, M. Moiroud, F. Guillocheau, and J.-F. Deconinck (2016), A
596 better-ventilated ocean triggered by Late Cretaceous changes in continental
597 configuration, *Nature communications*, *7*.
598 Dufresne, J. L., et al. (2013), Climate change projections using the IPSL-CM5 Earth
599 System Model: from CMIP3 to CMIP5, *Climate Dynamics*, *40*(9-10), 2123-2165.
600 Dunkley Jones, T., P. R. Bown, P. N. Pearson, B. S. Wade, H. K. Coxall, and C. H. Lear
601 (2008), Major shifts in calcareous phytoplankton assemblages through the Eocene‐
602 Oligocene transition of Tanzania and their implications for low‐latitude primary
603 production, *Paleoceanography*, *23*(4).
604 Eagles, G., and W. Jokat (2014), Tectonic reconstructions for paleobathymetry in Drake
605 Passage, *Tectonophysics*, *611*, 28-50.
606 Eagles, G., R. Livermore, and P. Morris (2006), Small basins in the Scotia Sea: the Eocene
607 Drake passage gateway, *Earth and Planetary Science Letters*, *242*(3), 343-353.
608 Egan, K. E., R. E. M. Rickaby, K. R. Hendry, and A. N. Halliday (2013), Opening the
609 gateways for diatoms primes Earth for Antarctic glaciation, *Earth and Planetary Science*
610 *Letters*, *375*, 34-43.
611 Elsworth, G., E. Galbraith, G. Halverson, and S. Yang (2017), Enhanced weathering and
612 CO2 drawdown caused by latest Eocene strengthening of the Atlantic meridional
613 overturning circulation, *Nature Geoscience*, *10*(3), 213-216.
614 England, M. H., D. K. Hutchinson, A. Santoso, and W. P. Sijp (2017), Ice-atmosphere
615 feedbacks dominate the response of the climate system to Drake Passage closure,
616 *Journal of Climate*(2017).
617 Erhardt, A. M., H. Pälike, and A. Paytan (2013), High‐resolution record of export
618 production in the eastern equatorial Pacific across the Eocene‐Oligocene transition
619 and relationships to global climatic records, *Paleoceanography*, *28*(1), 130-142.
620 Faul, K. L., and M. L. Delaney (2010), A comparison of early Paleogene export
621 productivity and organic carbon burial flux for Maud Rise, Weddell Sea, and Kerguelen
622 Plateau, south Indian Ocean, *Paleoceanography*, *25*(3).
623 Ferreira, D., J. Marshall, and J.-M. Campin (2010), Localization of deep water formation:
624 Role of atmospheric moisture transport and geometrical constraints on ocean
625 circulation, *Journal of Climate*, *23*(6), 1456-1476.
626 Fichefet, T., and M. A. Morales Maqueda (1997), Sensitivity of a global sea ice model to
627 the treatment of ice thermodynamics and dynamics, *Journal of Geophysical Research:*
628 *Oceans (1978–2012)*, *102*(C6), 12609-12646.
629 Fyke, J. G., M. D'Orgeville, and A. J. Weaver (2015), Drake Passage and Central American
630 Seaway controls on the distribution of the oceanic carbon reservoir, *Global and*
631 *Planetary Change*, *128*, 72-82.
632 Gasson, E., et al. (2014), Uncertainties in the modelled CO2 threshold for Antarctic
633 glaciation, *Climate of the Past*, *10*(2), 451-466.
634 Goldner, A., N. Herold, and M. Huber (2014), Antarctic glaciation caused ocean
635 circulation changes at the Eocene-Oligocene transition, *Nature*, *511*(7511), 574-577.
636 Griffith, E., M. Calhoun, E. Thomas, K. Averyt, A. Erhardt, T. Bralower, M. Lyle, A.
637 Olivarez‐Lyle, and A. Paytan (2010), Export productivity and carbonate accumulation
638 in the Pacific Basin at the transition from a greenhouse to icehouse climate (late Eocene
639 to early Oligocene), *Paleoceanography*, *25*(3).
640 Hain, M. P., D. M. Sigman, and G. H. Haug (2014), 8.18 The Biological Pump in the Past,
641 *Reference Module in Earth Systems and Environmental Sciences, Treatise on Geochemistry*,
642 485-517.

643 Heinze, C., and T. J. Crowley (1997), Sedimentary response to ocean gateway circulation
644 changes, *Paleoceanography*, *12*(6), 742-754.
645 Heureux, A. M. C., and R. E. M. Rickaby (2015), Refining our estimate of atmospheric CO2
646 across the Eocene–Oligocene climatic transition, *Earth and Planetary Science Letters*,
647 *409*, 329-338.
648 Hourdin, F., M.-A. Foujols, F. Codron, V. Guemas, J.-L. Dufresne, S. Bony, S. Denvil, L. Guez,
649 F. Lott, and J. Ghattas (2013), Impact of the LMDZ atmospheric grid configuration on the
650 climate and sensitivity of the IPSL-CM5A coupled model, *Climate Dynamics*, *40*(9-10),
651 2167-2192.
652 Huber, M., and D. Nof (2006), The ocean circulation in the southern hemisphere and its
653 climatic impacts in the Eocene, *Palaeogeography, Palaeoclimatology, Palaeoecology*,
654 *231*(1), 9-28.
655 Huber, M., L. C. Sloan, and C. Shellito (2003), Early Paleogene oceans and climate: A fully
656 coupled modeling approach using the NCAR CCSM, *Geological Society of America Special*
657 *Papers*, *369*, 25-47.
658 Huber, M., H. Brinkhuis, C. E. Stickley, K. Döös, A. Sluijs, J. Warnaar, S. A. Schellenberg,
659 and G. L. Williams (2004), Eocene circulation of the Southern Ocean: Was Antarctica
660 kept warm by subtropical waters?, *Paleoceanography*, *19*(4), PA4026.
661 John, E. H., P. N. Pearson, H. K. Coxall, H. Birch, B. S. Wade, and G. L. Foster (2013), Warm
662 ocean processes and carbon cycling in the Eocene, *Phil. Trans. R. Soc. A*, *371*(2001),
663 20130099.
664 Kageyama, M., et al. (2013), Mid-Holocene and Last Glacial Maximum climate
665 simulations with the IPSL model—part I: comparing IPSL_CM5A to IPSL_CM4, *Climate*
666 *Dynamics*, *40*(9-10), 2447-2468.
667 Katz, M. E., B. S. Cramer, J. R. Toggweiler, G. Esmay, C. Liu, K. G. Miller, Y. Rosenthal, B. S.
668 Wade, and J. D. Wright (2011), Impact of Antarctic Circumpolar Current Development on
669 Late Paleogene Ocean Structure, *Science*, *332*(6033), 1076-1079.
670 Kennett, J. P. (1977), Cenozoic evolution of Antarctic glaciation, the circum-Antarctic
671 Ocean, and their impact on global paleoceanography, *Journal of Geophysical Research*,
672 *82*(27), 3843-3860.
673 Krinner, G., N. Viovy, N. de Noblet‐Ducoudré, J. Ogée, J. Polcher, P. Friedlingstein, P.
674 Ciais, S. Sitch, and I. C. Prentice (2005), A dynamic global vegetation model for studies of
675 the coupled atmosphere‐biosphere system, *Global Biogeochemical Cycles*, *19*(1).
676 Ladant, J.-B., Y. Donnadieu, V. Lefebvre, and C. Dumas (2014), The respective role of
677 atmospheric carbon dioxide and orbital parameters on ice sheet evolution at the
678 Eocene-Oligocene transition, *Paleoceanography*, *29*(8), 810-823.
679 Lagabrielle, Y., Y. Goddéris, Y. Donnadieu, J. Malavieille, and M. Suarez (2009), The
680 tectonic history of Drake Passage and its possible impacts on global climate, *Earth and*
681 *Planetary Science Letters*, *279*(3-4), 197-211.
682 Le Mézo, P., L. Beaufort, L. Bopp, P. Braconnot, and M. Kageyama (2017), From monsoon
683 to marine productivity in the Arabian Sea: insights from glacial and interglacial climates,
684 *Climate of the Past*, *13*(7), 759-778.
685 Lear, C. H., and D. J. Lunt (2016), How Antarctica got its ice, *Science*, *352*(6281), 34-35.
686 Lear, C. H., H. Elderfield, and P. A. Wilson (2000), Cenozoic deep-sea temperatures and
687 global ice volumes from Mg/Ca in benthic foraminiferal calcite, *Science*, *287*(5451), 269-
688 272.
689 Lunt, D. J., P. J. Valdes, A. Haywood, and I. C. Rutt (2008), Closure of the Panama Seaway
690 during the Pliocene: implications for climate and Northern Hemisphere glaciation,
691 *Climate Dynamics*, *30*(1), 1-18.

692 Lunt, D. J., P. J. Valdes, T. D. Jones, A. Ridgwell, A. M. Haywood, D. N. Schmidt, R. Marsh,
693 and M. Maslin (2010), CO2-driven ocean circulation changes as an amplifier of
694 Paleocene-Eocene thermal maximum hydrate destabilization, *Geology*, *38*(10), 875-878.
695 Madec, G. (2008), NEMO ocean engine. Technical note.*Rep.*, IPSL.
696 Madec, G., and M. Imbard (1996), A global ocean mesh to overcome the North Pole
697 singularity, *Climate Dynamics*, *12*(6), 381-388.
698 Mariotti, V., L. Bopp, A. Tagliabue, M. Kageyama, and D. Swingedouw (2012), Marine
699 productivity response to Heinrich events: a model-data comparison, *Climate of the Past*,
700 *8*(5), 1581.
701 Matthews, R. K., and R. Z. Poore (1980), Tertiary δ 18O record and glacio-eustatic sea-
702 level fluctuations, *Geology*, *8*(10), 501-504.
703 Merico, A., T. Tyrrell, and P. A. Wilson (2008), Eocene/Oligocene ocean de-acidification
704 linked to Antarctic glaciation by sea-level fall, *Nature*, *452*(7190), 979-982.
705 Mikolajewicz, U., E. Maier-Reimer, T. J. Crowley, and K.-Y. Kim (1993), Effect of Drake
706 and Panamanian gateways on the circulation of an ocean model, *Paleoceanography*, *8*(4),
707 409-426.
708 Miller, K. G., J. D. Wright, and R. G. Fairbanks (1991), Unlocking the ice house:
709 Oligocene‐Miocene oxygen isotopes, eustasy, and margin erosion, *Journal of*
710 *Geophysical Research: Solid Earth*, *96*(B4), 6829-6848.
711 Moore, T. C., B. S. Wade, T. Westerhold, A. M. Erhardt, H. K. Coxall, J. Baldauf, and M.
712 Wagner (2014), Equatorial Pacific productivity changes near the Eocene‐Oligocene
713 boundary, *Paleoceanography*, *29*(9), 825-844.
714 Munday, D. R., H. L. Johnson, and D. P. Marshall (2015), The role of ocean gateways in the
715 dynamics and sensitivity to wind stress of the early Antarctic Circumpolar Current,
716 *Paleoceanography*, *30*(3), 284-302.
717 Nilsen, E. B., L. D. Anderson, and M. L. Delaney (2003), Paleoproductivity, nutrient burial,
718 climate change and the carbon cycle in the western equatorial Atlantic across the
719 Eocene/Oligocene boundary, *Paleoceanography*, *18*(3).
720 Pagani, M., M. Huber, Z. Liu, S. M. Bohaty, J. Henderiks, W. Sijp, S. Krishnan, and R. M.
721 DeConto (2011), The Role of Carbon Dioxide During the Onset of Antarctic Glaciation,
722 *Science*, *334*(6060), 1261-1264.
723 Pälike, H., et al. (2012), A Cenozoic record of the equatorial Pacific carbonate
724 compensation depth, *Nature*, *488*(7413), 609-614.
725 Pearson, P. N., G. L. Foster, and B. S. Wade (2009), Atmospheric carbon dioxide through
726 the Eocene–Oligocene climate transition, *Nature*, *461*(7267), 1110-1113.
727 Plancq, J., E. Mattioli, B. Pittet, L. Simon, and V. Grossi (2014), Productivity and sea-
728 surface temperature changes recorded during the late Eocene–early Oligocene at DSDP
729 Site 511 (South Atlantic), *Palaeogeography, Palaeoclimatology, Palaeoecology*, *407*, 34-
730 44.
731 Salamy, K. A., and J. C. Zachos (1999), Latest Eocene–Early Oligocene climate change and
732 Southern Ocean fertility: inferences from sediment accumulation and stable isotope
733 data, *Palaeogeography, Palaeoclimatology, Palaeoecology*, *145*(1), 61-77.
734 Sarmiento, J. L., N. Gruber, M. A. Brzezinski, and J. P. Dunne (2004), High-latitude
735 controls of thermocline nutrients and low latitude biological productivity, *Nature*,
736 *427*(6969), 56-60.
737 Scher, H., and E. Martin (2006), Timing and climatic consequences of the opening of
738 Drake Passage, *Science*, *312*(5772), 428-430.

739 Scher, H., J. M. Whittaker, S. E. Williams, J. C. Latimer, W. E. Kordesch, and M. L. Delaney
740 (2015), Onset of Antarctic Circumpolar Current 30 million years ago as Tasmanian
741 Gateway aligned with westerlies, *Nature*, *523*(7562), 580-583.
742 Schumacher, S., and D. Lazarus (2004), Regional differences in pelagic productivity in
743 the late Eocene to early Oligocene—a comparison of southern high latitudes and lower
744 latitudes, *Palaeogeography, palaeoclimatology, palaeoecology*, *214*(3), 243-263.
745 Séférian, R., et al. (2016), Inconsistent strategies to spin up models in CMIP5:
746 implications for ocean biogeochemical model performance assessment, *Geoscientific*
747 *Model Development*, *9*(5), 1827-1851.
748 Sepulchre, P., T. Arsouze, Y. Donnadieu, J. C. Dutay, C. Jaramillo, J. Le Bras, E. Martin, C.
749 Montes, and A. J. Waite (2014), Consequences of shoaling of the Central American
750 Seaway determined from modeling Nd isotopes, *Paleoceanography*, *29*(3), 176-189.
751 Siesser, W. G. (1995), Paleoproductivity of the Indian Ocean during the Tertiary period,
752 *Global and Planetary Change*, *11*(1-2), 71-88.
753 Sijp, W. P., and M. H. England (2004), Effect of the Drake Passage throughflow on global
754 climate, *Journal of physical oceanography*, *34*(5), 1254-1266.
755 Sijp, W. P., and M. H. England (2005), Role of the Drake Passage in controlling the
756 stability of the ocean's thermohaline circulation, *Journal of climate*, *18*(12), 1957-1966.
757 Sijp, W. P., M. H. England, and J. R. Toggweiler (2009), Effect of ocean gateway changes
758 under greenhouse warmth, *Journal of Climate*, *22*(24), 6639-6652.
759 Sijp, W. P., M. H. England, and M. Huber (2011), Effect of the deepening of the Tasman
760 Gateway on the global ocean, *Paleoceanography*, *26*(4), PA4207.
761 Stickley, C. E., H. Brinkhuis, S. A. Schellenberg, A. Sluijs, U. Röhl, M. Fuller, M. Grauert, M.
762 Huber, J. Warnaar, and G. L. Williams (2004), Timing and nature of the deepening of the
763 Tasmanian Gateway, *Paleoceanography*, *19*(4), PA4027
764 Tagliabue, A., O. Aumont, and L. Bopp (2014), The impact of different external sources of
765 iron on the global carbon cycle, *Geophysical Research Letters*, *41*(3), 920-926.
766 Takahashi, T., W. S. Broecker, and S. Langer (1985), Redfield ratio based on chemical
767 data from isopycnal surfaces, *Journal of Geophysical Research: Oceans*, *90*(C4), 6907-
768 6924.
769 Tan, N., G. Ramstein, C. Dumas, C. Contoux, J.-B. Ladant, P. Sepulchre, Z. Zhang, and S. De
770 Schepper (2017), Exploring the MIS M2 glaciation occurring during a warm and high
771 atmospheric CO2 Pliocene background climate, *Earth and Planetary Science Letters*, *472*,
772 266-276.
773 Toggweiler, J., and H. Bjornsson (2000), Drake Passage and palaeoclimate, *Journal of*
774 *Quaternary Science*, *15*(4), 319-328.
775 Toggweiler, J. R., and B. Samuels (1993), New radiocarbon constraints on the upwelling
776 of abyssal water to the ocean's surface., in *The global carbon cycle.*, edited by M.
777 Heimann, pp. 333-366, Springer, Berlin, Heidelberg.
778 Valcke, S. (2006), OASIS user's guide (prism-2.5). Tech. Rep. TR/CMGC/06/73, PRISM
779 Report No3.*Rep.*, CERFACS, Toulouse, France.
780 Villa, G., C. Fioroni, D. Persico, A. P. Roberts, and F. Florindo (2014), Middle Eocene to
781 Late Oligocene Antarctic glaciation/deglaciation and southern ocean productivity,
782 *Paleoceanography*, *29*(3), 223-237.
783 Winguth, A. M. E., E. Thomas, and C. Winguth (2012), Global decline in ocean ventilation,
784 oxygenation, and productivity during the Paleocene-Eocene Thermal Maximum:
785 Implications for the benthic extinction, *Geology*, *40*(3), 263-266.
786 Yang, S., E. Galbraith, and J. Palter (2014), Coupled climate impacts of the Drake Passage
787 and the Panama Seaway, *Climate Dynamics*, *43*(1-2), 37-52.

Zachos, J. C., and L. R. Kump (2005), Carbon cycle feedbacks and the initiation of Antarctic glaciation in the earliest Oligocene, *Global and Planetary Change*, *47*(1), 51-66.
Zhang, Z.-S., Q. Yan, and H.-J. Wang (2010), Has the Drake passage played an essential role in the Cenozoic cooling, *Atmos. Oceanic Sci. Lett*, *3*(5), 288-292.

Legends and Tables

Site (Reference)	Latitude	Longitude	Qualitative productivity change
1209-1211 (Griffith et al. 2010)	~ 20°N	~ 172°W	decrease
925 (Nilsen et al. 2003) *	~ 4°N	~ 43°W	no change
U1333 (Moore et al. 2014)	~ 3°N	~ 113°W	decrease
1218 and U1334 (Moore et al. 2014)	~ 0-2°N	~ 110°W	decrease
462 (Schumacher and Lazarus 2004)	~ 2°S	~ 178°W	no change
959 (Schumacher and Lazarus 2004)	~ 2°S	~ 13°W	slight decrease or no change
574 (Schumacher and Lazarus 2004)	~ 7°S	~ 117°W	slight decrease or no change
709 (Siesser 1995)	~ 10°S	~ 75°E	decrease
758 (Siesser 1995)	~ 10°S	~ 110°E	no change or no data
757 (Siesser 1995)	~ 30°S	~ 95°E	no change
762 (Siesser 1995)	~ 35°S	~ 115°E	decrease
763 (Diester-Haas and Zahn 2001)	~ 40°S	~ 112°E	increase
1090 (Diekmann et al. 2004)	~ 43°S	~ 9°E	decrease
1090 (Egan et al. 2013)	~ 43°S	~ 9°E	increase
752 (Siesser 1995)	~ 45°S	~ 90°E	no change or no data
511 (Plancq et al. 2014)	~ 52°S	~ 42°W	increase
511 (Schumacher and Lazarus 2004)	~ 55°S	~ 42°W	increase
748 (Siesser 1995)	~ 55°S	~ 70°E	no change or no data
592 (Diester-Haas and Zahn 2001)	~ 55°S	~ 165°E	increase
748 (Schumacher and Lazarus 2004)	~ 56°S	~ 73°E	increase
748 (Villa et al. 2014)	~ 57°S	~ 74°E	increase
738 and 744 (Villa et al. 2014) *	~ 63°S	~ 83°E	increase
689 (Schumacher and Lazarus 2004)	~ 72°S	~ 15°W	increase
689 and 690 (Villa et al. 2014)	~ 72°S	~ 15°W	increase

Table 1. Compilation of long-term productivity changes across the late Eocene and early Oligocene. Longitudes and latitudes are approximate paleolocations of the sites. The asterisk denotes sites where modern location is used. There are a few redundant sites but findings from different studies at these sites are similar.

Figure 1. (top) Mean annual export production at 100 m ($gC.m^{-2}.yr^{-1}$) for DC and DO simulations. (bottom) Annual export production at 100 m difference between DO and DC ($gC.m^{-2}.yr^{-1}$). Color-coded circles represent productivity variations from data records (see Table 1): red = increase, blue = decrease, pale shading = weak or uncertain variations, white = no variations or lack of data.

Figure 2. Zonally averaged export production at 100 m ($gC.m^{-2}.yr^{-1}$) at the global scale and in each basin for DC (black solid lines) and DO (red dashed lines).

Figure 3. (top) Mean annual zonally averaged nitrate concentration ($\mu mol.L^{-1}$) for DC and DO with density contours (0.1 $kg.m^{-3}$) overlain. (bottom) Mean annual zonally averaged nitrate concentration difference ($\mu mol.L^{-1}$) between DO and DC, with density contours (0.1 $kg.m^{-3}$) overlain in black for DC and green for DO. Note that 1000 $kg.m^{-3}$ is subtracted from density values on the plot.

Figure 4. Global, Atlantic, Pacific and Indian upper 500 m nitrate concentration gradients in the low latitudes (40°S – 40°N, solid lines) and the southern high latitudes (90°S – 60°S, dashed lines) for DC (black) and DO (red).

Figure 5. Global meridional overturning streamfunction (Sv, clockwise positive) for DC and DO. Contours 4 Sv, negative dashed.

Figure 6. Wintertime deep-water formation in the Southern (top) and Northern (bottom) Hemispheres for DF and DO simulations, as represented by the ocean mixed-layer depth (m). Note that the scale differs between southern and northern plots.

Figure 7. Diatoms and nanophytoplankton primary production difference ($gC.m^{-2}.yr^{-1}$) between DO and DC.

Figures

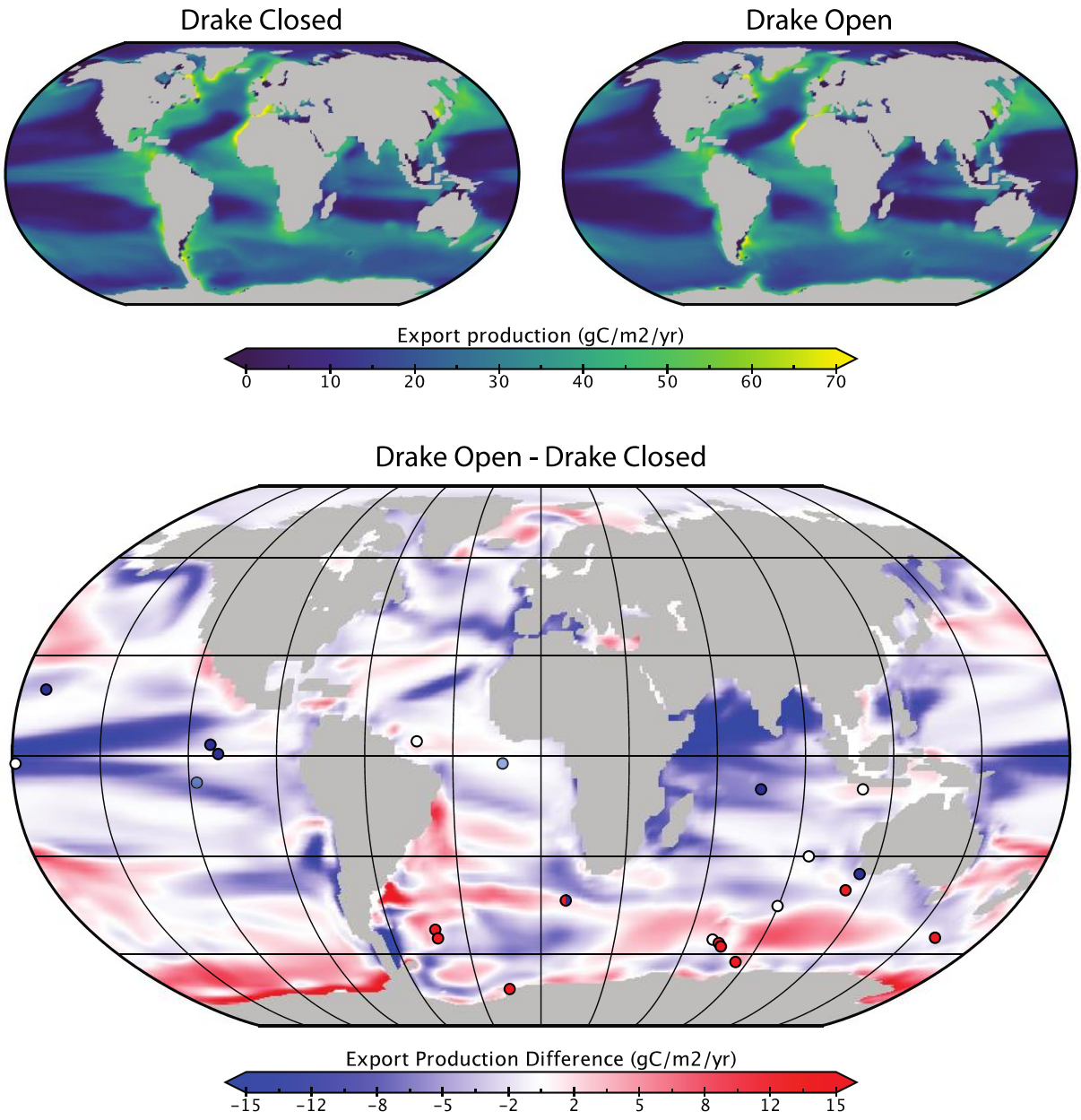

Figure 1.

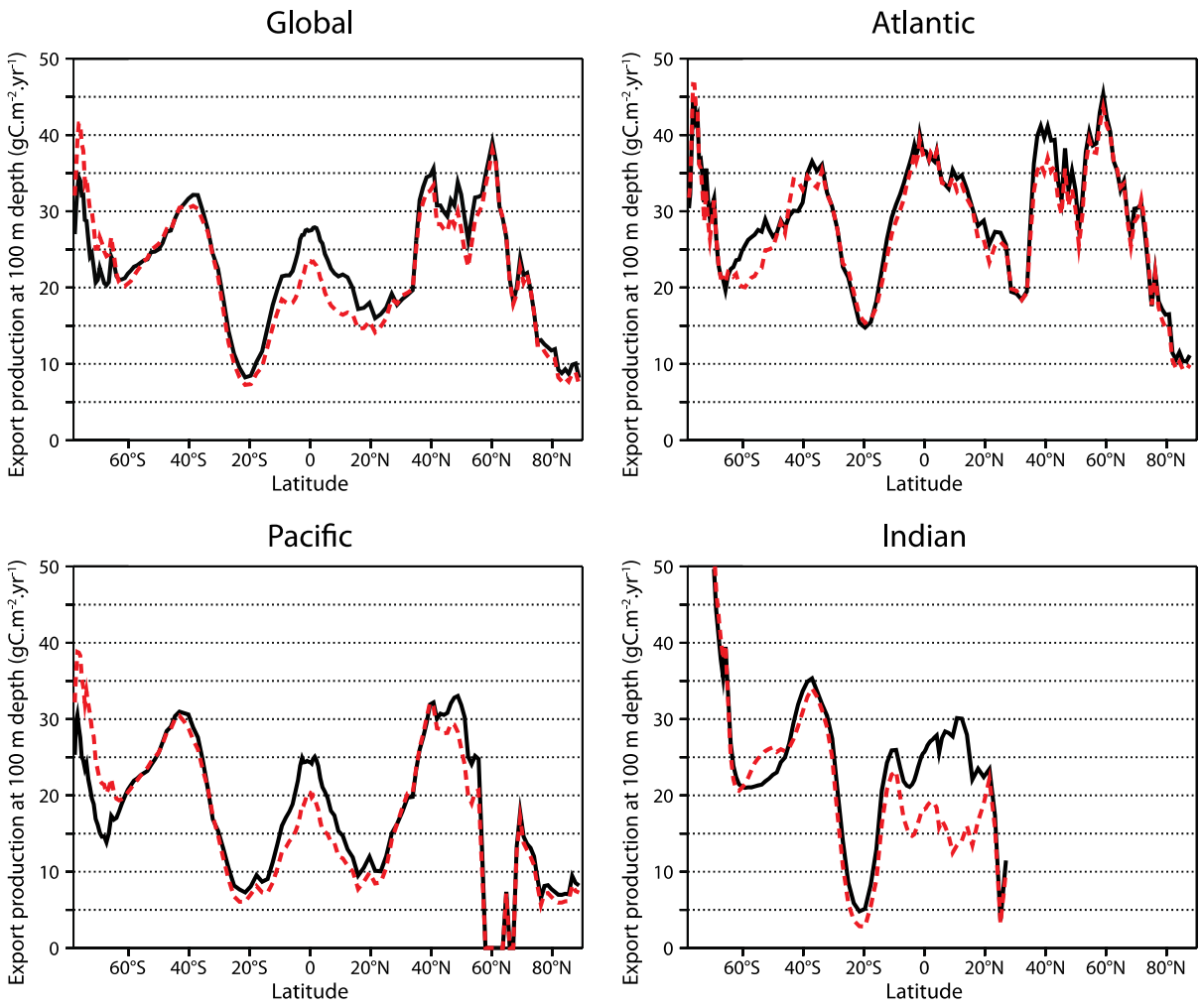
Global
Atlantic
Pacific
Indian
Export production at 100 m depth (gC.m-2.yr-1)
0
10
20
30
40
50
60°S
40°S
20°S
0
20°N
40°N
60°N
80°N
Latitude

Figure 2.

841

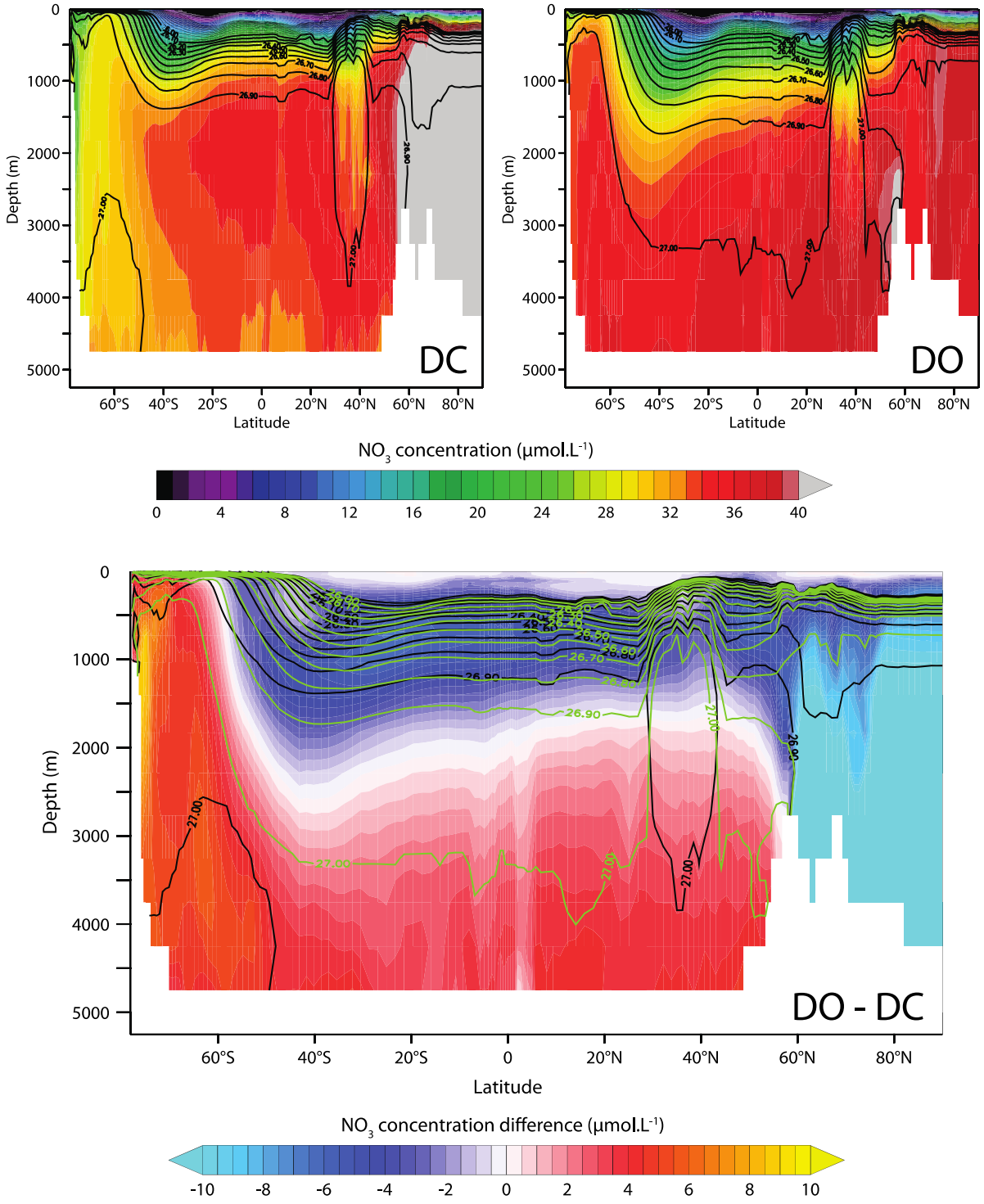
DC
DO
DO - DC
Depth (m)
Latitude
60°S 40°S 20°S 0 20°N 40°N 60°N 80°N
0 1000 2000 3000 4000 5000
NO3 concentration (µmol.L-1)
0 4 8 12 16 20 24 28 32 36 40
NO3 concentration difference (µmol.L-1)
-10 -8 -6 -4 -2 0 2 4 6 8 10

Figure 3.

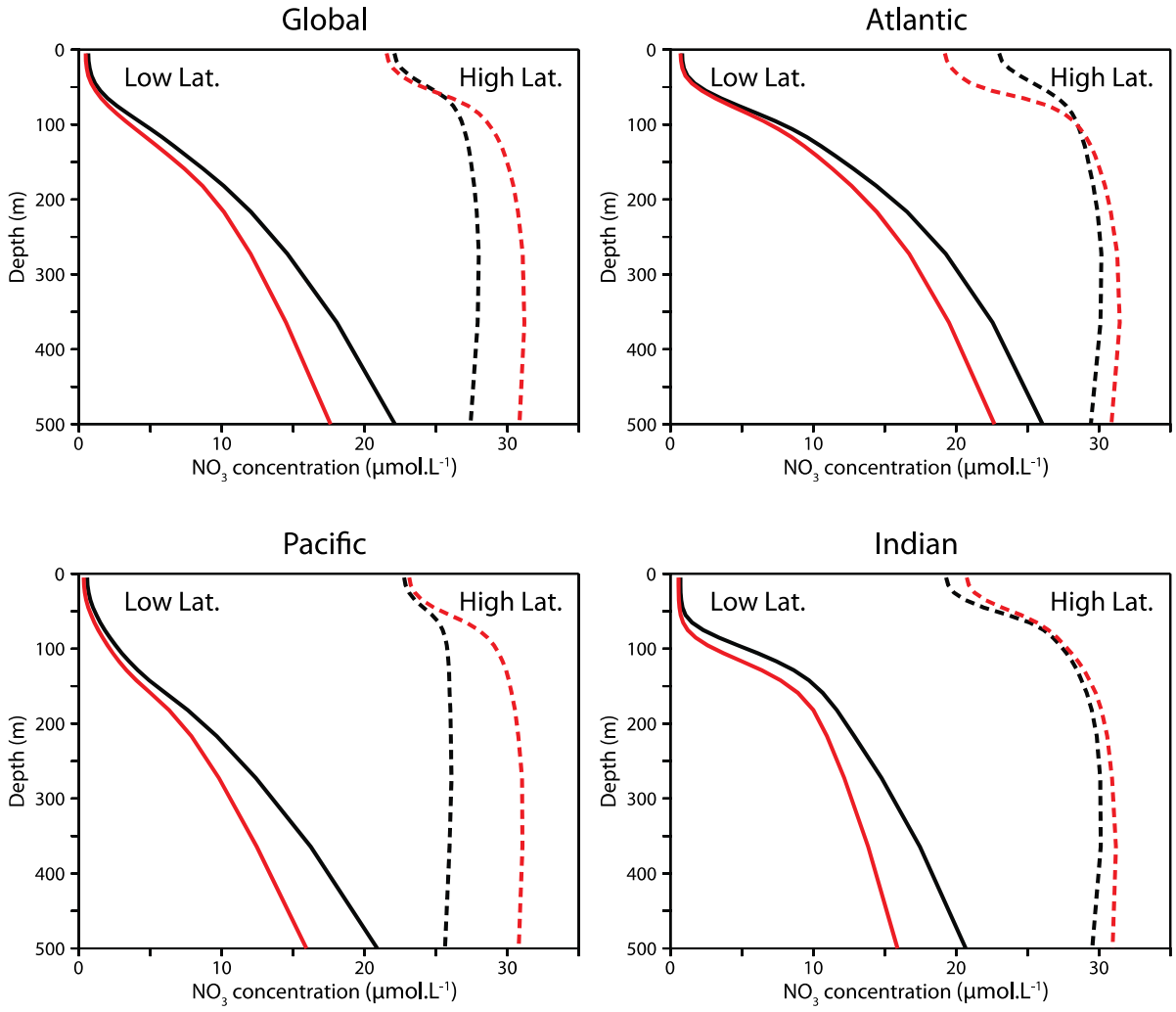
Global
Atlantic
Pacific
Indian
Low Lat.
High Lat.
Depth (m)
0
100
200
300
400
500
0
10
20
30
NO3 concentration (µmol.L-1)

Figure 4.

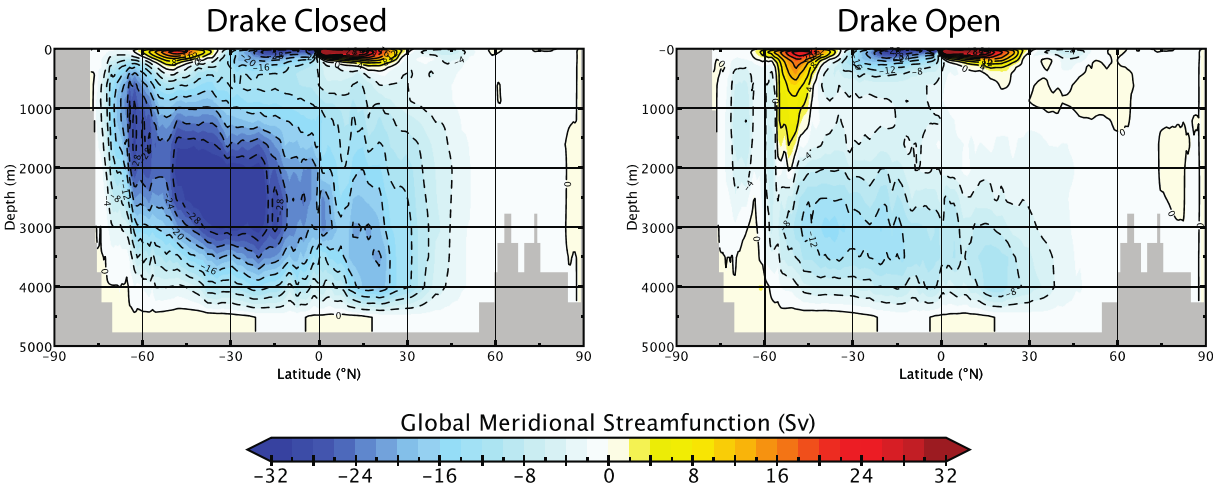
Drake Closed
Drake Open
Depth (m)
Latitude (°N)
Global Meridional Streamfunction (Sv)
−32
−24
−16
−8
0
8
16
24
32

Figure 5.

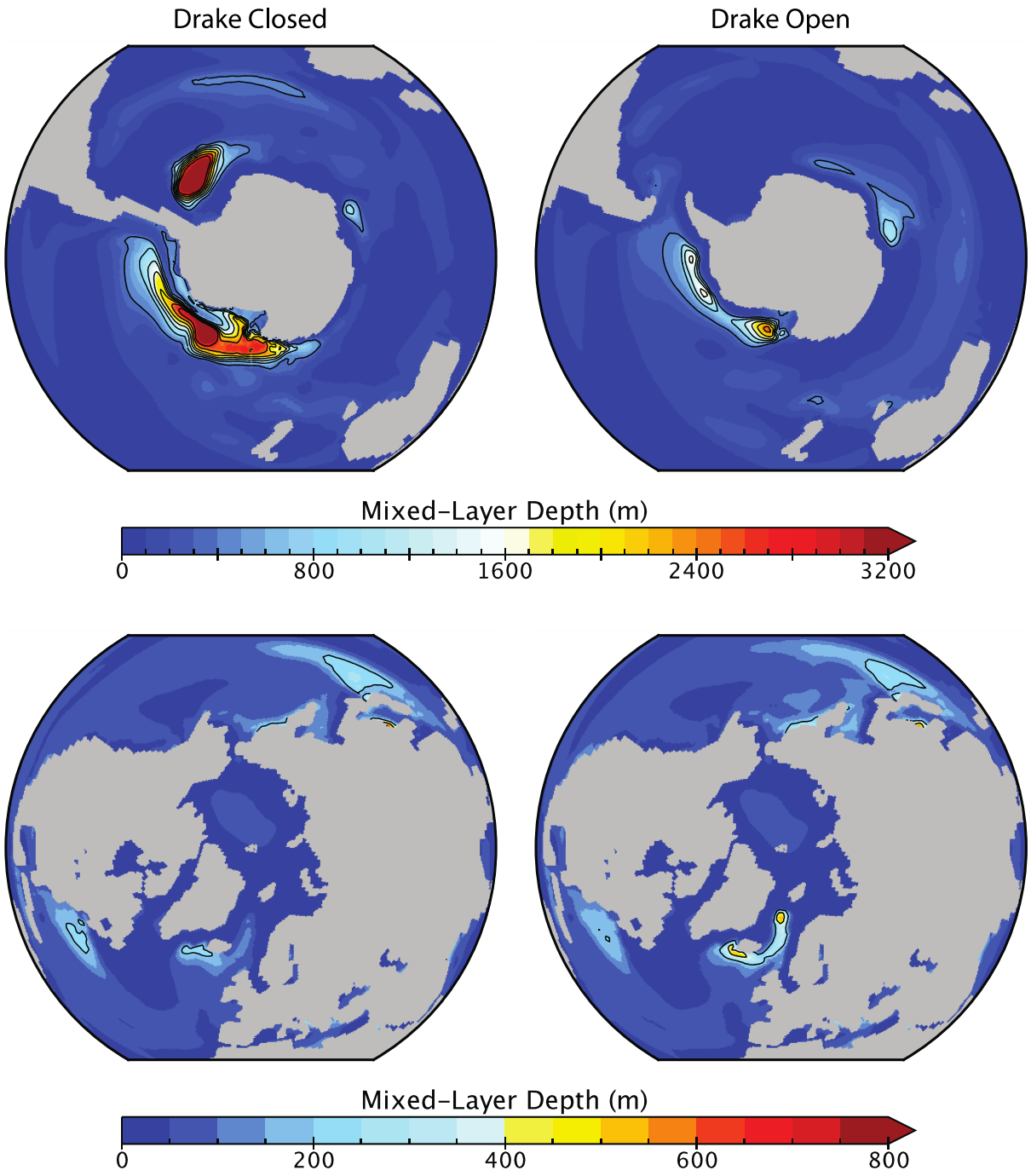
Drake Closed
Drake Open
Mixed-Layer Depth (m)
0
800
1600
2400
3200
Mixed-Layer Depth (m)
0
200
400
600
800

Figure 6.

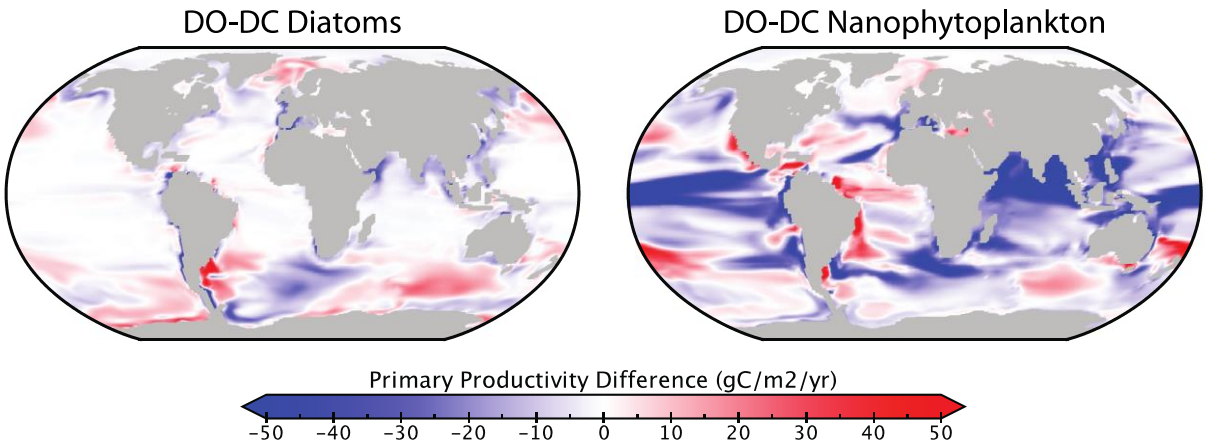

Figure 7.

878

879

880